ACS Energy LETTERS

http://pubs.acs.org/journal/aelccp

Polaron-Based Electronic Conduction in Mixed Ionic-Electronic Conducting Lithium Garnets

Charles E. Schwarz, Ramanuja Srinivasan Saravanan, Nina M. Borodin, Yunsheng Liu, Eric D. Wachsman, and Yifei Mo*

Cite This: *ACS Energy Lett.* 2024, 9, 5334−5340

Read Online

ACCESS | Metrics & More | Article Recommendations | Supporting Information

ABSTRACT: Recent research has demonstrated that doped lithium garnet compositions with mixed ionic−electronic conducting (MIEC) properties can significantly enhance the performance of solid-state batteries with lithium metal anodes. However, the mechanisms that enable electronic conduction in these garnets are not well understood. In this study, we conduct first-principles calculations to investigate the polaron-based mechanism of electronic conduction in these MIEC garnets. We model polaron trapping on multivalent cation dopants in the lithium garnet structure and estimate the energy barriers for site-to-site polaron migration. By analyzing defect formation energies and cation charge transitions, we elucidate why certain cations and cation combinations greatly enhance the electronic conductivity in lithium garnets. Our computations lead to suggestions for new cation dopants and new strategies to further improve MIEC garnets in high-performance solid-state batteries. The study can serve as a general framework to guide the further development of novel MIEC materials for energy technologies.

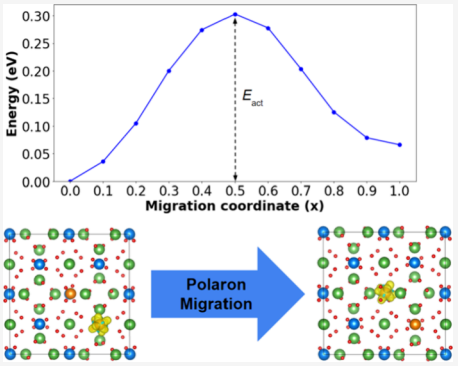

In recent years, solid-state batteries (SSBs) have received a great deal of attention as the next generation of Li-ion battery technology. In place of the organic liquid electrolyte used in traditional Li-ion batteries, SSBs use a Li-conducting solid material as the electrolyte, offering improved safety and enabling the use of a lithium metal anode, which would significantly increase Li-ion battery energy densities.[1,2] Lithium garnets with the general formula of $Li_xA_3B_2O_{12}$, and particularly the doped variants of $Li_7La_3Zr_2O_{12}$ (LLZO), have been considered as some of the most promising solid electrolyte materials, thanks to their high Li-ion conductivity and chemical stability with Li metal.[3−5] Researchers have addressed the high interfacial resistance at the garnet−anode interface through interface engineering techniques such as applying a metal oxide interlayer between the garnet and Li,[6−8] or using a three-dimensional (3D) porous−dense−porous trilayer architecture with Li metal infiltrated into the garnet porous framework,[9,10] enabling the construction of high-performing cells using a garnet solid electrolyte with a Li metal anode. Recently, Alexander et al. designed and demonstrated a series of doped Li garnet compositions with mixed ionic and electronic conducting (MIEC) properties by substituting different multivalent cations, such as Pr, Ce, Nb, Nd, and Cr, into LLZO.[11] A prototype SSB with the trilayer architecture constructed using these MIEC garnet compositions demonstrated exceptional Li-metal cycling stability and capacity and achieved an order of magnitude increase in critical current density for this structure at room temperature with no applied pressure.[11] These high-rate results are believed to be due to the electron and Li-ion conducting pathways provided by the MIEC garnets, which enable uniform plating of Li metal across the entire porous garnet layer surface rather than being limited to triple phase boundaries where Li ions conducting through the garnet meet electrons, initially from the current collector and then the moving Li metal boundary in the pore structure.

The origin of electronic conductivity in MIEC garnets is not well understood, as pure LLZO is a wide-bandgap material with electronic conductivity on the order of 10^{-9} S/cm.[12−14] In previous computational studies, Squires et al. investigated the formation energies and concentrations of various defects under aliovalent doping in tetragonal LLZO[15] and explained the low concentrations and mobility of charge carriers in LLZO, leading to low electronic conductivity.[13]

This computational study investigates the hypothesis that the electronic conductivity in these new MIEC garnets originates from the migration of small polarons. Polarons are

Received: July 29, 2024
Revised: September 7, 2024
Accepted: October 7, 2024
Published: October 10, 2024

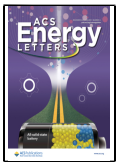

https://doi.org/10.1021/acsenergylett.4c02060
ACS Energy Lett. 2024, 9, 5334−5340

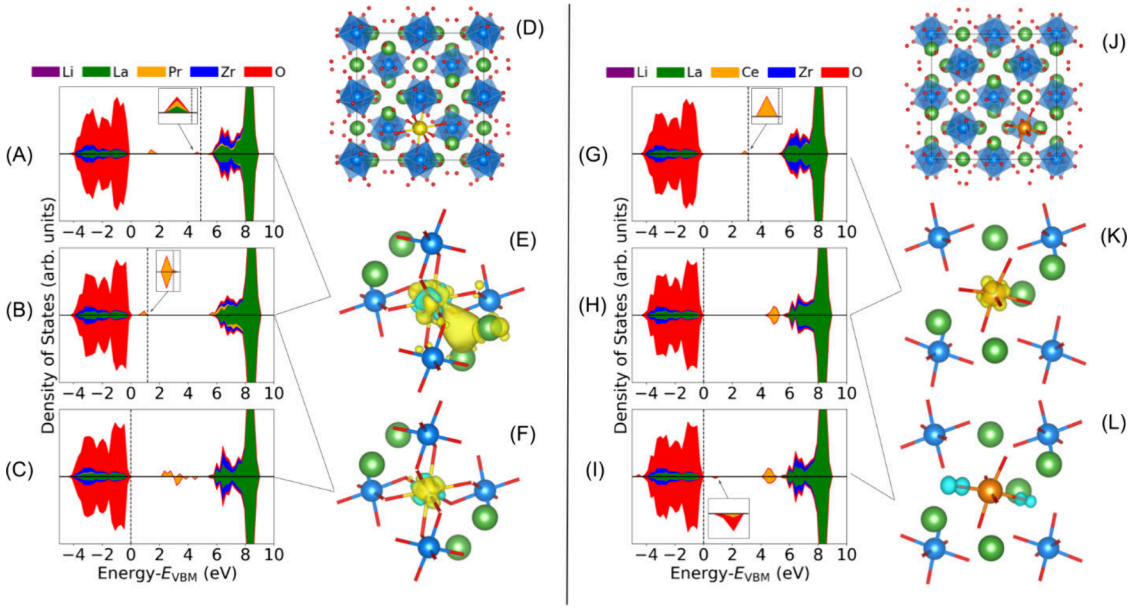

Figure 1. (A−C) HSE06 DOS for the 1Pr-LLZO supercell with (A) one excess electron, (B) no excess charge carriers, and (C) one excess hole. (D) The atomic structure of the 1Pr-LLZO supercell. (E) The isosurface of differential spin density between states A and B, showing the electron polaron localized among Pr and two La atoms. (F) The isosurface of differential spin density between states B and C, showing the hole polaron localized on Pr. (G−I) HSE06 DOS for the 1Ce-LLZO supercell with (G) one excess electron, (H) no excess charge carriers, and (I) one excess hole. (J) The atomic structure of the 1Ce-LLZO supercell. (K) The isosurface of differential spin density between states G and H, showing the electron polaron localized on Ce. (L) The isosurface of differential spin density between states H and I, showing the hole polaron localized on the CeO_6 octahedron. The vertical dashed line in the DOS indicates the highest occupied state. Each colored section represents that element's contribution to the total DOS. The isosurfaces for plots E, F, K, and L are at 2%, 5%, 5%, and 15% of the maximum values, respectively, with positive values in yellow and negative values in blue.

charge carriers that become self-trapped in a material structure associated with distortion of the surrounding lattice.[16,17] Polaron migration has been reported as a key electronic conduction mechanism in a variety of oxide materials, e.g., $Li_xMn_2O_4$,[18] TiO_2,[19,20] CeO_2,[21] $SrCeO_3$,[22] and $CaMnO_{3-\delta}$,[23] which are used in a range of applications such as batteries, catalysts, membranes, and fuel cells. While previous work has suggested the existence of small polarons in Li garnets,[24,25] it remains unclear exactly what types of polarons may form, how they migrate, how they are affected by different cations, and particularly why these new compositions of MIEC garnets can achieve such high electronic conductivities. To understand how polarons provide increased electronic conductivity in these novel doped MIEC garnets, we perform first-principles calculations to examine the formation and migration of polarons, evaluate the defect chemistries and conditions affecting the polaron formation, and computationally predict new dopants that could contribute to the MIEC behavior in Li garnets.

Polaron Formation. Our calculations are based on the screened hybrid Heyd−Scuseria−Ernzerhof (HSE06) functional,[26−28] which has been commonly adopted for modeling the localization of polarons[20,22,29] and demonstrated to accurately reproduce the lattice structures and band gaps of LLZO (SI).[12,15,25] Details about the computational methods are provided in the Supporting Information (SI).

The novel MIEC garnets are achieved by substituting different multivalent cations, such as Pr, Ce, Nb, Nd, and Cr, into LLZO.[11] These multivalent cation dopants are expected to induce the polaron formation in LLZO, as observed in other oxide materials.[17,22,29] In order to have polaron-based electronic conduction, the cation dopant should have the ability to trap polarons and the polarons should have high mobilities and high concentration in the structure. We first investigated the formation of polarons due to Pr and Ce substituted on La and Zr sites,[30−32] respectively, in LLZO, as these were key multivalent cations in the MIEC garnet produced by Alexander et al.[11] Following Kroger−Vink notation, A_B denotes the substitution of species A located on a B site.[33] Supercell models with a single Pr_{La} and Ce_{Zr} substitution in cubic LLZO (denoted 1Pr-LLZO and 1Ce-LLZO, respectively) were constructed (see Methods in the SI). To investigate the formation of electron or hole polarons in the doped garnet structures, an electron was added or removed from the 1Pr-LLZO or 1Ce-LLZO supercell models, and the structure was subsequently relaxed. The formation of the polaron was confirmed by inspecting changes in the element-projected partial density of states (PDOS). The localization of the polaron in space was visualized by calculating the spin density, which is the difference between the spin-up and spin-down electron densities for the relaxed structures. The differential spin density is defined as the difference in spin density between two electronic states (Figure 1).

In the 1Pr-LLZO supercell, the excess hole localizes directly on the Pr site (Figure 1F), indicating that the Pr oxidation state effectively transitions from +3 to +4, forming a hole polaron. This transition may be expected, as +3 and +4 are known oxidation states for Pr. With the formation of this hole polaron, the average Pr−O bond length decreases from 2.52 to 2.40 Å. When an excess electron is added to the supercell, it is shared between the Pr site and two adjacent La sites (Figure 1F), and the average Pr−O bond length increases to 2.57 Å. This isosurface is similar to the one observed by Demir et al. in pure cubic-phase LLZO, where an electron polaron is shared

https://doi.org/10.1021/acsenergylett.4c02060
ACS Energy Lett. 2024, 9, 5334−5340

between three La sites.[25] It is unclear whether the electron localized among three cations is physically accurate, given the DFT's known tendency to delocalize electrons. The observed defect state of Pr in the DOS may align with previous observations that Pr-substituted garnets exhibit color changes.[30]

In the 1Ce-LLZO supercell, the excess electron forms a polaron localized on the Ce site (Figure 1K). The localization of this electron on the Ce site means the Ce oxidation state transitions from +4 to +3, and the average Ce−O bond length increases from 2.21 to 2.36 Å. Similar polaron-related transitions between the Ce^{3+} and Ce^{4+} states have been observed in CeO_2 and $SrCeO_3$.[21,22] The excess hole is shared by the oxygen in the CeO_6 octahedron (Figure 1L), similar to the configuration previously reported in $SrCeO_3$,[22] with the average Ce−O bond length decreasing to 2.19 Å. The shared distribution of trapped charge on multiple O sites is also observed in $BaTiO_3$,[34] Li_2O_2,[35] and $KNbO_3$.[36]

In addition to Pr_{La} and Ce_{Zr}, a variety of other multivalent cations substitutions in the LLZO structure were investigated (Nd_{La}, Sm_{La}, Nb_{Zr}, Sn_{Zr}, Ti_{Zr}, Cr_{Zr}, W_{Zr}, Mo_{Zr}, and Fe_{Li}). These dopants were selected based on the previous experimental studies[3,11,30,37,38] and the low values of the energy above the convex hull (E_{hull}) suggesting good phase stabilities for these doped garnet structures (see the SI). The preferred sites for these dopants were chosen based on a previous analysis by Miara et al.[32] The results of first-principles calculations for the polaron formation on these substitutions are provided in the SI and demonstrate that many of these dopants are capable of forming polarons. For these polarons to significantly contribute to the electronic conductivity, high mobility and high concentrations are also required as evaluated later.

Polaron Migration. To yield electronic conductivity, the polarons formed on these multivalent cations should have a high mobility to migrate from site to site through the material's crystal structure. High polaron mobility requires a low energy barrier for site-to-site polaron hopping.[16,39,40] Here, we calculate the energy barrier for polaron migration using the approach implemented by Maxisch and colleagues[41] (see the SI).

For a hole polaron migrating between two adjacent Pr_{La} sites, the calculated energy barrier is 0.18 eV (Figure 2A). This

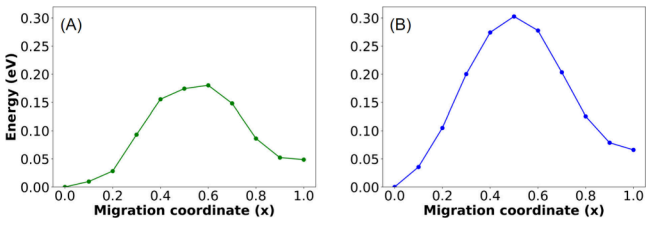

Figure 2. Energy barrier profiles for (A) the migration of a hole polaron between two Pr sites and (B) the migration of an electron polaron between two Ce sites.

value is comparable to the reported barrier in other materials that exhibit mobile polarons.[19,29,41] Since the $(Pr,La)O_8$ polyhedra are connected through edge-sharing, there are many pathways for this migration to occur across the garnet structure, especially in a garnet where Pr fully substituted La, as in the experiments by Alexander et al.[11]

For polaron migration between two Ce_{Zr} sites, the calculated energy barrier is 0.30 eV (Figure 2B). However, Ce/Zr sites are separated by 5.63 Å and the $(Ce,Zr)O_6$ octahedra are not connected through shared edges or corners. We expect the polarons cannot directly hop between two Ce sites and would require the polaron to occupy a La-site cation or Li-site cation (e.g., Fe) as an intermediate state. Our attempt to model a polaron migration from a Ce site to a Pr site was not successful due to the preferred localization of the polaron on Ce sites (SI).

Defect Energies. Having high electronic conductivity will require both high polaron mobility and high polaron concentration, which is determined by the polarons' formation energies and their interactions with other defects in the garnet at the given equilibrium conditions.[15] Using the procedure described in the SI, we evaluated the formation energies of Li vacancies (V_{Li}), Li interstitials (Li_i), and O vacancies (V_O), in several garnet compositions: (A) pure cubic LLZO, (B) LLZO with a single Pr_{La} substitution, and (C) LLZO with a single Ce_{Zr} substitution and an additional Li, which is the energetically favorable composition in equilibrium with Li metal (SI). We also evaluated the formation energy associated with adding an extra electron or an extra hole to the model, which could either form a polaron or become delocalized throughout the supercell. For these calculations, the lithium chemical potential was set to be in equilibrium with Li metal ($\Delta\mu_{Li} = 0$), and the oxygen chemical potential was set to $\Delta\mu_O = -4.83$ eV based on the stability region of LLZO determined by Squires et al.[15,42] Figure 3 displays the computed formation energies as a function of the Fermi level. The calculated formation energies for vacancies and interstitials are in good agreement with previous results for tetragonal and cubic LLZO.[15,25] In our calculation, an excess hole added to the pure LLZO supercell became delocalized rather than forming a polaron.

The formation energies of charged defects are dependent on the Fermi level (Figure 3), which is dependent on the processing and operating conditions of the material. While determining the self-consistent Fermi level requires considering all possible defects in self-consistent evaluation,[43] it can be approximated by the intersection of the most dominant defects, which are V_{Li} and Li_i in these Li garnets.[15,25] This gives an approximate Fermi level in the range of 4.8 to 5.0 eV above the valence band maximum (VBM).

The most notable difference between the three garnets is the formation energy associated with excess charge carriers. In Figure 3C, the formation energy for the hole polaron (i.e., the transition from Ce^{3+} to Ce^{4+}) is 0.8 eV in the estimated Fermi level range. In the Pr-doped LLZO, the hole polaron is more energetically favorable than that in undoped LLZO, indicating improved charge trapping capabilities of multivalent Pr. The low formation energies of polarons in the doped garnet structures indicate that these materials will contain a high concentration of polarons, which is required to achieve a high electronic conductivity by polaron-based mechanisms.

Dopant Transition Levels. In addition to showing the formation energy of polarons as a function of the Fermi level (Figure 3), the charge transition levels are a simple and intuitive way to show the most favorable oxidation states of the dopant as a function of the Fermi level, and the distance between the transition level and the Fermi level is the formation energy. We calculated and plotted the charge transition levels for a wide range of cation dopants in LLZO (Figure 4, Table S4). The different regions in the transition level diagram (Figure 4) indicate the most stable oxidation

https://doi.org/10.1021/acsenergylett.4c02060
ACS Energy Lett. 2024, 9, 5334−5340

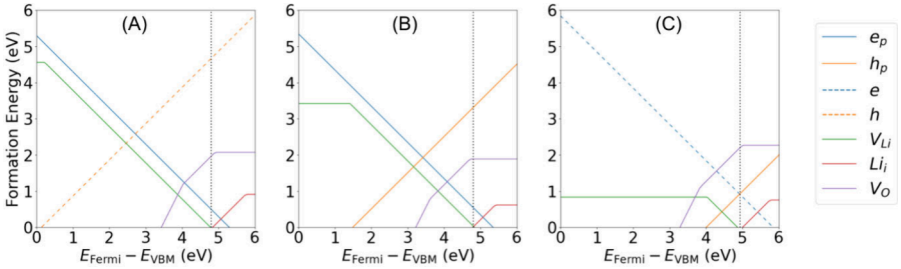

Figure 3. Defect formation energy diagrams for (A) pure cubic LLZO, (B) LLZO with a single Pr_{Zr} substitution in the supercell, and (C) LLZO with a single Ce_{Zr} substitution and an additional Li atom intercalated in the supercell. The formation energies are evaluated under Li-rich and O-poor conditions using the chemical potentials $\Delta\mu_{Li} = 0$ and $\Delta\mu_O = -4.83$ eV referenced to the calculated pure elements in their standard state (see SI). The vertical, black, dotted line indicates the estimated Fermi energy E_{Fermi} referenced to the VBM as 0. Dashed lines indicate the formation energy for a delocalized electron or hole, for cases where polarons did not localize around a single cation site.

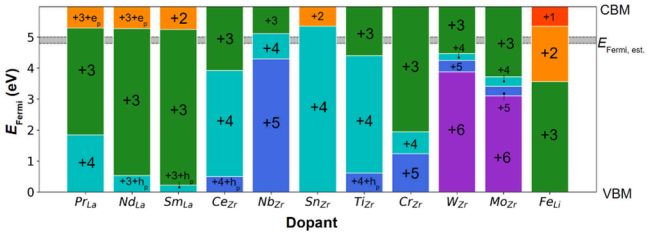

Figure 4. Charge transition levels for various dopants in LLZO. The colored regions in the diagram indicate the most stable oxidation state at the given Fermi level. Numerical labels denote the oxidation state of the dopant atom (as inferred from DOS and spin density), h_p denotes a hole polaron localized on the oxygen atoms surrounding the dopant atom, and e_p denotes an electron polaron localized between the dopant and two La atoms. Gray shaded region in the background gives the estimated Fermi level range of 4.8 to 5.0 eV.

state for the dopant at a certain Fermi level. For a doped garnet with the Fermi level near a transition level between two oxidation states, there is a lower formation energy for the dopant to transition between oxidation states, i.e., forming a polaron. As indicated in Figure 4, the estimated Fermi level range of 4.8−5.0 eV is near the transition levels of several multivalent dopants including Ce_{Zr}. Therefore, a high concentration of Ce polarons, i.e., a mixture of Ce^{3+} and Ce^{4+}, is expected. Other multivalent dopants, such as Nb_{Zr}, Ti_{Zr}, and Fe_{Li}, also have charge transition levels near the Fermi levels, indicating that low formation energies and high polaron concentrations are expected in the garnet with these cation dopants. These findings agree with the previous experimental report of electronic conduction in Li garnets doped with Nb, Ti, or Fe.[11,14,24,37] Therefore, as shown by first-principles computation, having cation dopants that have the appropriate charge transition levels is crucial for achieving high carrier concentrations and providing electronic conductivity. The computation also predicts W and Mo as promising dopants for forming polarons in Li garnets (Figure 4).

Our results on polaron formation and migration provide insight on how certain cation dopants in MIEC garnets can enable electronic conductivity. Furthermore, the combinations of multiple dopants substituted into these garnets may lead to a high electronic conductivity, as observed in previous experiments. For example, in the case of MIEC $Li_{6.4}Ga_{0.2}Pr_3Zr_{1.8}Ce_{0.2}O_{12}$ reported by Alexander et al.,[11] the substitution of the multivalent cation species Pr and Ce on La and Zr sites, respectively, may have a synergistic effect in increasing electronic conductivity. Substituting Pr on all La sites creates a well-connected network of possible polaron sites (green arrows in Figure 5). The substitution of Ce in this

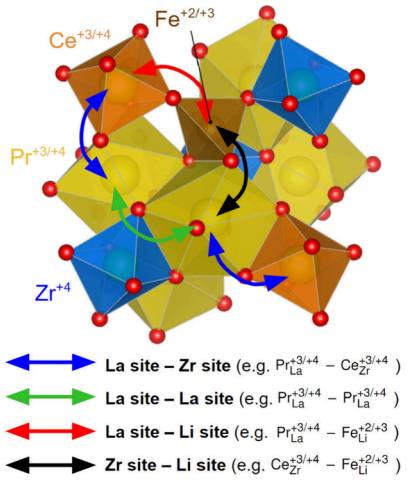

Figure 5. Proposed pathways for polaron hopping between different multivalent dopants in the garnet structure. Arrows indicate possible hops between different cation/dopant sites. The 3D-connected pathways are formed among Pr_{La} (green arrow) and can be further connected by Ce_{Zr} (blue arrow) and Fe_{Li} (red/black arrow). (Polyhedra color keys: Pr_{La}, yellow; Zr, blue; Ce_{Zr}, orange; Fe_{Li}, brown; and O, red.)

garnet would be expected to produce a high concentration of hole polarons due to the appropriate transition levels of Ce_{Zr}. Furthermore, thanks to the polaron formation on Ce, Ce provides additional polaron hopping pathways (blue arrows in Figure 5) to further facilitate the polaron migration in the garnet structures (SI). Therefore, having multiple multivalent cation substitutions, such as Ce_{Zr} or Nb_{Zr}, in tandem with Pr_{La}, increases the polaron concentration and also facilitates polaron migration. Both a high polaron concentration and well-connected polaron migration pathways (Figure 5) are essential for achieving higher electronic conductivities as in these double-doped MIEC garnets.[11] Transition level calculations indicate that other dopants, such as Ti, Mo, or W, on the Zr site can play a role similar to that of Ce in increasing the polaron concentration. Similarly, multivalent cations substituted on Li sites, such as Fe_{Li}, could also promote polaron formation as shown in the transition level diagram (Figure 4) and connect polaron migration pathways through the Li sites (red arrows in Figure 5), which would explain the high electronic conductivity reported for Fe-doped LLZO.[24] In

https://doi.org/10.1021/acsenergylett.4c02060
ACS Energy Lett. 2024, 9, 5334−5340

summary, having multiple multivalent cations enables a variety of pathways for polaron migration. Figure 5 illustrates the potential pathways for polaron migration by connecting different dopant sites in the garnet structure. Additionally, as shown by molecular dynamics simulations, these MIEC garnets with a variety of dopant substitutions maintain high Li-ion conductivities (SI). To further increase the electronic conductivity in MIEC garnets, one may choose the dopant species that further increase polaron concentrations and produce higher polaron mobilities. Another proposed strategy is triple-doping these garnets by introducing multivalent cations simultaneously on La, Zr, and Li sites to further promote polaron formation and connected migration pathways.

Further studies are needed to understand the polaron migrations between different dopant species that may occur in these garnet structures (SI). Understanding the effects of Li disordering and defect binding energy on polaron formation and migration is also necessary. To obtain more accurate values of polaron energies with different dopants, the functionals beyond HSE06 may be tested and compared.[44] The finite-size corrections for the polaronic states may also be evaluated.[45] Estimating the Fermi level in the corresponding synthesis or processing conditions of these new garnets would also require more comprehensive studies.[15,25] All of the above are required to give a reliable quantification of the electronic conductivity given by the polarons mechanisms.

In summary, these first-principles calculations demonstrate that multivalent cation dopants facilitate the formation of polarons in lithium garnets. Additionally, these polarons have reasonably low energy barriers for migration and low formation energies, meaning that they will have high mobility and high concentrations, respectively. These results support the idea that small polaron migration plays a key role in producing electronic conductivity in these novel MIEC lithium garnets. By analyzing how different dopant atoms affect polaronic behavior and conductivity in garnet structures, we predict new dopant species and strategies that can improve the MIEC properties of these garnets, leading to further improvements in SSB performance.[11] Beyond lithium garnets, our computational work provides general guidance for understanding the influence of different dopants on polaron behavior and for the rational design of new materials with MIEC properties. This study demonstrates how first-principles computational techniques can serve as a valuable tool to understand and predict polaronic mechanisms in MIEC materials and to design MIEC materials targeted toward important applications, such as battery electrodes, solid oxide fuel cells, solid oxide electrolyzers, and membranes for gas separation.

■ ASSOCIATED CONTENT

Supporting Information

The Supporting Information is available free of charge at https://pubs.acs.org/doi/10.1021/acsenergylett.4c02060.

Computational methods; element-resolved density of states for other doped LLZO; phase stability (E_{hull}) of doped LLZO; computation results on Li-ion conductivities of doped LLZO; Li stoichiometry in Ce-doped LLZO; dopant transition levels; comments on electron and hole polaron migration (PDF)

■ AUTHOR INFORMATION

Corresponding Author

Yifei Mo − *Department of Materials Science and Engineering, University of Maryland, College Park, Maryland 20742, United States; Maryland Energy Innovation Institute, University of Maryland, College Park, Maryland 20742, United States;* orcid.org/0000-0002-8162-4629; Email: yfmo@umd.edu

Authors

Charles E. Schwarz − *Department of Materials Science and Engineering, University of Maryland, College Park, Maryland 20742, United States*

Ramanuja Srinivasan Saravanan − *Department of Materials Science and Engineering, University of Maryland, College Park, Maryland 20742, United States*

Nina M. Borodin − *Department of Materials Science and Engineering, University of Maryland, College Park, Maryland 20742, United States;* orcid.org/0009-0004-4670-4991

Yunsheng Liu − *Department of Materials Science and Engineering, University of Maryland, College Park, Maryland 20742, United States*

Eric D. Wachsman − *Department of Materials Science and Engineering, University of Maryland, College Park, Maryland 20742, United States; Maryland Energy Innovation Institute, University of Maryland, College Park, Maryland 20742, United States;* orcid.org/0000-0002-0667-1927

Complete contact information is available at: https://pubs.acs.org/10.1021/acsenergylett.4c02060

Notes

The authors declare no competing financial interest.

■ ACKNOWLEDGMENTS

We acknowledge the funding support from the Center for Research in Extreme Batteries (CREB) under the Cooperative Agreement (CA) Number W911NF-22-2-0021. The views and conclusions contained in this document are those of the authors and should not be interpreted as representing the official policies of the U.S. Government. We acknowledge the computational facilities from the University of Maryland supercomputing resources.

■ REFERENCES

(1) Janek, J.; Zeier, W. G. A Solid Future for Battery Development. *Nat. Energy* **2016**, *1*, 16141.

(2) Albertus, P.; Babinec, S.; Litzelman, S.; Newman, A. Status and Challenges in Enabling the Lithium Metal Electrode for High-Energy and Low-Cost Rechargeable Batteries. *Nat. Energy* **2018**, *3*, 16−21.

(3) Thangadurai, V.; Narayanan, S.; Pinzaru, D. Garnet-Type Solid-State Fast Li Ion Conductors for Li Batteries: Critical Review. *Chem. Soc. Rev.* **2014**, *43*, 4714−4727.

(4) Wang, C.; Fu, K.; Kammampata, S. P.; McOwen, D. W.; Samson, A. J.; Zhang, L.; Hitz, G. T.; Nolan, A. M.; Wachsman, E. D.; Mo, Y.; Thangadurai, V.; Hu, L. Garnet-Type Solid-State Electrolytes: Materials, Interfaces, and Batteries. *Chem. Rev.* **2020**, *120* (10), 4257.

(5) Zhu, Y.; He, X.; Mo, Y. Origin of Outstanding Stability in the Lithium Solid Electrolyte Materials: Insights from Thermodynamic Analyses Based on First-Principles Calculations. *ACS Appl. Mater. Interfaces* **2015**, *7* (42), 23685−23693.

(6) Fu, K. K.; Gong, Y.; Liu, B.; Zhu, Y.; Xu, S.; Yao, Y.; Luo, W.; Wang, C.; Lacey, S. D.; Dai, J.; Chen, Y.; Mo, Y.; Wachsman, E.; Hu, L. Toward Garnet Electrolyte-Based Li Metal Batteries: An Ultrathin,

Highly Effective, Artificial Solid-State Electrolyte/Metallic Li Interface. *Sci. Adv.* **2017**, *3* (4), No. e1601659.
(7) Han, X.; Gong, Y.; Fu, K.; He, X.; Hitz, G. T.; Dai, J.; Pearse, A.; Liu, B.; Wang, H.; Rubloff, G.; Mo, Y.; Thangadurai, V.; Wachsman, E. D.; Hu, L. Negating Interfacial Impedance in Garnet-Based Solid-State Li Metal Batteries. *Nat. Mater.* **2017**, *16* (5), 572−579.
(8) Lou, J.; Wang, G.; Xia, Y.; Liang, C.; Huang, H.; Gan, Y.; Tao, X.; Zhang, J.; Zhang, W. Achieving Efficient and Stable Interface between Metallic Lithium and Garnet-Type Solid Electrolyte through a Thin Indium Tin Oxide Interlayer. *J. Power Sources* **2020**, *448*, 227440.
(9) Hitz, G. T.; McOwen, D. W.; Zhang, L.; Ma, Z.; Fu, Z.; Wen, Y.; Gong, Y.; Dai, J.; Hamann, T. R.; Hu, L.; Wachsman, E. D. High-Rate Lithium Cycling in a Scalable Trilayer Li-Garnet-Electrolyte Architecture. *Mater. Today* **2019**, *22*, 50−57.
(10) Xu, S.; McOwen, D. W.; Wang, C.; Zhang, L.; Luo, W.; Chen, C.; Li, Y.; Gong, Y.; Dai, J.; Kuang, Y.; Yang, C.; Hamann, T. R.; Wachsman, E. D.; Hu, L. Three-Dimensional, Solid-State Mixed Electron-Ion Conductive Framework for Lithium Metal Anode. *Nano Lett.* **2018**, *18* (6), 3926−3933.
(11) Alexander, G. V.; Shi, C.; O'Neill, J.; Wachsman, E. D. Extreme Lithium-Metal Cycling Enabled by a Mixed Ion- and Electron-Conducting Garnet Three-Dimensional Architecture. *Nat. Mater.* **2023**, *22*, 1136−1143.
(12) Thompson, T.; Yu, S.; Williams, L.; Schmidt, R. D.; Garcia-Mendez, R.; Wolfenstine, J.; Allen, J. L.; Kioupakis, E.; Siegel, D. J.; Sakamoto, J. Electrochemical Window of the Li-Ion Solid Electrolyte Li7La3Zr2O12. *ACS Energy Lett.* **2017**, *2* (2), 462.
(13) Squires, A. G.; Davies, D. W.; Kim, S.; Scanlon, D. O.; Walsh, A.; Morgan, B. J. Low Electronic Conductivity of Li7La3Zr2 O12 Solid Electrolytes from First Principles. *Phys. Rev. Mater.* **2022**, *6*, 085401.
(14) Cheng, X.; Huang, J.; Qiang, W.; Huang, B. Synthesis of Mixed Ionic and Electronic Conducting Garnet with Doping of Transition Elements (Fe, Co, Ni). *Ceram. Int.* **2020**, *46* (3), 3731−3737.
(15) Squires, A. G.; Scanlon, D. O.; Morgan, B. J. Native Defects and Their Doping Response in the Lithium Solid Electrolyte Li7La3Zr2O12. *Chem. Mater.* **2020**, *32* (5), 1876−1886.
(16) Emin, D. *Polarons*; Cambridge University Press: Cambridge, 2013.
(17) Franchini, C.; Reticcioli, M.; Setvin, M.; Diebold, U. Polarons in Materials. *Nat. Rev. Mater.* **2021**, *6*, 560−586.
(18) Ouyang, C.; Du, Y.; Shi, S.; Lei, M. Small Polaron Migration in LixMn2O4: From First Principles Calculations. *Physics Letters, Section A: General, Atomic and Solid State Physics* **2009**, *373* (31), 2796−2799.
(19) Carey, J. J.; Quirk, J. A.; McKenna, K. P. Hole Polaron Migration in Bulk Phases of TiO_2 Using Hybrid Density Functional Theory. *J. Phys. Chem. C* **2021**, *125* (22), 12441−12450.
(20) Deák, P.; Aradi, B.; Frauenheim, T. Polaronic Effects in TiO2 Calculated by the HSE06 Hybrid Functional: Dopant Passivation by Carrier Self-Trapping. *Phys. Rev. B Condens Matter Mater. Phys.* **2011**, *83*, 155207.
(21) Tuller, H. L.; Nowick, A. S. Small Polaron Electron Transport in Reduced CeO2 Single Crystals. *J. Phys. Chem. Solids* **1977**, *38* (8), 859−867.
(22) Bai, Q.; Zhu, Y.; He, X.; Wachsman, E.; Mo, Y. First Principles Hybrid Functional Study of Small Polarons in Doped SrCeO3 Perovskite: Towards Computation Design of Materials with Tailored Polaron. *Ionics (Kiel)* **2018**, *24*, 1139−1151.
(23) Schrade, M.; Kabir, R.; Li, S.; Norby, T.; Finstad, T. G. High Temperature Transport Properties of Thermoelectric CaMnO 3-δ - Indication of Strongly Interacting Small Polarons. *J. Appl. Phys.* **2014**, *115*, 103705.
(24) Jin, Z.; Kong, X.; Huang, H.; Jiang, Y.; Xiang, W.; Xu, Y.; Zhang, L.; Peng, R.; Wang, C. Garnet-Type Solid-State Mixed Ionic and Electronic Conductor. *Energy Storage Mater.* **2023**, *59*, 102788.
(25) Demir, S.; Tekin, A.; Chan, Y. Te; Scheurer, C.; Reuter, K.; Luntz, A. C.; Voss, J. Factors Affecting the Electron Conductivity in Single Crystal Li7La3Zr2O12 and Li7P3S11. *ACS Appl. Energy Mater.* **2024**, *7* (6), 2392−2404.
(26) Heyd, J.; Scuseria, G. E.; Ernzerhof, M. Hybrid Functionals Based on a Screened Coulomb Potential. *J. Chem. Phys.* **2003**, *118*, 8207−8215.
(27) Heyd, J.; Scuseria, G. E.; Ernzerhof, M. Erratum: Hybrid Functionals Based on a Screened Coulomb Potential (Journal of Chemical Physics (2003) 118 (8207)). *J. Chem. Phys.* **2006**, *124*, 219906.
(28) Paier, J.; Marsman, M.; Hummer, K.; Kresse, G.; Gerber, I. C.; Angyán, J. G. Screened Hybrid Density Functionals Applied to Solids. *J. Chem. Phys.* **2006**, *124*, 154709.
(29) Wu, F.; Ping, Y. Combining Landau-Zener Theory and Kinetic Monte Carlo Sampling for Small Polaron Mobility of Doped BiVO4 from First-Principles. *J. Mater. Chem. A Mater.* **2018**, *6* (41), 20025−20036.
(30) Wang, C.; Ping, W.; Bai, Q.; Cui, H.; Hensleigh, R.; Wang, R.; Brozena, A. H.; Xu, Z.; Dai, J.; Pei, Y.; Zheng, C.; Pastel, G.; Gao, J.; Wang, X.; Wang, H.; Zhao, J. C.; Yang, B.; Zheng, X.; Luo, J.; Mo, Y.; Dunn, B.; Hu, L. A General Method to Synthesize and Sinter Bulk Ceramics in Seconds. *Science (1979)* **2020**, *368* (6490), 521−526.
(31) Dong, B.; Yeandel, S. R.; Goddard, P.; Slater, P. R. Combined Experimental and Computational Study of Ce-Doped La3Zr2Li7O12 Garnet Solid-State Electrolyte. *Chem. Mater.* **2020**, *32* (1), 215−223.
(32) Miara, L. J.; Richards, W. D.; Wang, Y. E.; Ceder, G. First-Principles Studies on Cation Dopants and Electrolyte|Cathode Interphases for Lithium Garnets. *Chem. Mater.* **2015**, *27* (11), 4040−4047.
(33) Kröger, F. A.; Vink, H. J. Relations between the Concentrations of Imperfections in Crystalline Solids. *Solid State Physics - Advances in Research and Applications* **1956**, *3* (C), 307−435.
(34) Possenriede, E.; Jacobs, P.; Schirmer, O. F. Paramagnetic Defects in BaTiO3 and Their Role in Light-Induced Charge Transport. I. ESR Studies. *J. Phys.: Condens. Matter* **1992**, *4* (19), 4719−4742.
(35) Ong, S. P.; Mo, Y.; Ceder, G. Low Hole Polaron Migration Barrier in Lithium Peroxide. *Phys. Rev. B Condens Matter Mater. Phys.* **2012**, *85*, No. 081105(R).
(36) Kotomin, E. A.; Eglitis, R. I.; Postnikov, A. V.; Borstel, G.; Christensen, N. E. First-Principles and Semiempirical Calculations for Bound-Hole Polarons in KNbO3. *Phys. Rev. B Condens Matter Mater. Phys.* **1999**, *60* (1), 1.
(37) Gao, J.; Zhu, J.; Li, X.; Li, J.; Guo, X.; Li, H.; Zhou, W. Rational Design of Mixed Electronic-Ionic Conducting Ti-Doping Li7La3Zr2O12 for Lithium Dendrites Suppression. *Adv. Funct Mater.* **2021**, *31*, 2001918.
(38) Samson, A. J.; Hofstetter, K.; Bag, S.; Thangadurai, V. A Bird's-Eye View of Li-Stuffed Garnet-Type Li7La3Zr2O12 Ceramic Electrolytes for Advanced All-Solid-State Li Batteries. *Energy Environ. Sci.* **2019**, *12* (10), 2957−2975.
(39) Marcus, R. A. Electron Transfer Reactions in Chemistry. Theory and Experiment. *Rev. Mod. Phys.* **1993**, *65* (3), 599.
(40) Holstein, T. Studies of Polaron Motion. Part II. The "Small" Polaron. *Ann. Phys. (N Y)* **1959**, *8* (3), 343−389.
(41) Maxisch, T.; Zhou, F.; Ceder, G. Ab Initio Study of the Migration of Small Polarons in Olivine Lix FePO4 and Their Association with Lithium Ions and Vacancies. *Phys. Rev. B Condens Matter Mater. Phys.* **2006**, *73*, 104301.
(42) Squires, A. G.; Scanlon, D. O.; Morgan, B. J. GitHub repository containing analysis for "Native Defects and their Doping Response in the Lithium Solid Electrolyte $Li_7La_3Zr_2O_{12}$. https://github.com/alexsquires/native-defects-in-llzo (accessed October 4, 2024).
(43) Buckeridge, J. Equilibrium Point Defect and Charge Carrier Concentrations in a Material Determined through Calculation of the Self-Consistent Fermi Energy. *Comput. Phys. Commun.* **2019**, *244*, 329−342.
(44) Miceli, G.; Chen, W.; Reshetnyak, I.; Pasquarello, A. Nonempirical Hybrid Functionals for Band Gaps and Polaronic Distortions in Solids. *Phys. Rev. B* **2018**, *97*, No. 121112(R).

https://doi.org/10.1021/acsenergylett.4c02060
ACS Energy Lett. 2024, 9, 5334−5340

(45) Chen, W.; Pasquarello, A. Correspondence of Defect Energy Levels in Hybrid Density Functional Theory and Many-Body Perturbation Theory. *Phys. Rev. B Condens Matter Mater. Phys.* **2013**, *88*, 115104.

https://doi.org/10.1021/acsenergylett.4c02060
ACS Energy Lett. 2024, 9, 5334−5340